Entanglement Generated by Dissipation and Steady State Entanglement of Two Macroscopic Objects

Hanna Krauter,[1] Christine A. Muschik,[2] Kasper Jensen,[1] Wojciech Wasilewski,[1,*] Jonas M. Petersen,[1] J. Ignacio Cirac,[2] and Eugene S. Polzik[1,†]

[1]*Niels Bohr Institute, Danish Quantum Optics Center QUANTOP, Copenhagen University, Copenhagen, Denmark*
[2]*Max-Planck-Institut für Quantenoptik, Garching, Germany*

(Received 15 April 2011; published 17 August 2011)

Entanglement is a striking feature of quantum mechanics and an essential ingredient in most applications in quantum information. Typically, coupling of a system to an environment inhibits entanglement, particularly in macroscopic systems. Here we report on an experiment where dissipation continuously generates entanglement between two macroscopic objects. This is achieved by engineering the dissipation using laser and magnetic fields, and leads to robust event-ready entanglement maintained for 0.04 s at room temperature. Our system consists of two ensembles containing about 10^{12} atoms and separated by 0.5 m coupled to the environment composed of the vacuum modes of the electromagnetic field. By combining the dissipative mechanism with a continuous measurement, steady state entanglement is continuously generated and observed for up to 1 h.

DOI: 10.1103/PhysRevLett.107.080503 PACS numbers: 03.67.Bg, 03.65.Ud, 03.67.Hk, 42.50.−p

To date, experiments investigating quantum superpositions and entanglement are hampered by decoherence. Its effects have been studied in several systems [1]. However, it was recognized [2] that the engineered interaction with a reservoir can drive the system into a desired steady state. In particular, dissipation common for two systems can drive them into an entangled state [3]. The idea of using and engineering dissipation rather than relying on coherent evolutions only represents a paradigm shift with potentially significant practical advantages. Contrary to other methods, entanglement generation by dissipation does not require the preparation of a system in a particular input state and exists, in principle, for an arbitrary long time, which is expected to play an important role in quantum information protocols [4–7]. These features make dissipative methods inherently stable against weak random perturbations, with the dissipative dynamics stabilizing the entanglement.

We report on the first demonstration of purely dissipative entanglement generation [8]. In contrast to previous approaches [9–11], entanglement is obtained without using measurements on the quantum state of the environment (i.e., the light field). The dissipation-based method implemented here is deterministic and unconditional and therefore fundamentally different from standard approaches such as the quantum-nondemolition-based method [9] or the Duan-Lukin-Cirac-Zoller (DLCZ) protocol [4], which yield a separable state if the emitted photons are not detected. Furthermore, we report the creation of a steady state atomic entanglement by combining the dissipative mechanism proposed in [12] with continuous measurements. The generated entanglement is of the EPR type, which plays a central role in continuous variable quantum information processing [6,13], quantum sensing [14], and metrology [11,15,16].

Figure 1(a) presents the principles of engineered dissipation in our system consisting of two ^{133}Cs ensembles, interacting with a y-polarized laser field at ω_L. A pair of two-level systems is encoded in the $6S_{1/2}$ ground state sublevels $|\uparrow\rangle_{\mathrm{I}} \equiv |4,4\rangle_{\mathrm{I}}$, $|\downarrow\rangle_{\mathrm{I}} \equiv |4,3\rangle_{\mathrm{I}}$, and $|\uparrow\rangle_{\mathrm{II}} \equiv |4,-3\rangle_{\mathrm{II}}$, $|\downarrow\rangle_{\mathrm{II}} \equiv |4,-4\rangle_{\mathrm{II}}$. Operators $J^{\pm}_{\mathrm{I,II}}$ with $J^- = \sum_{i=1}^{N} |\uparrow\rangle_i\langle\downarrow|$ describe collective spin flips, where N is the number of atoms. The atoms are placed in a magnetic field in the x direction and the collective operators $J_y = \sqrt{2}(J^+ + J^-)$ and $J_z = i\sqrt{2}(J^+ - J^-)$ are defined in the frame rotating at the Larmor frequency Ω. The two ensembles are initialized by optical pumping along the x axis in the extreme states $m_F = 4$ and $m_F = -4$, respectively, corresponding to $\langle J_x\rangle \equiv \langle J_{x,\mathrm{I}}\rangle = -\langle J_{x,\mathrm{II}}\rangle \approx 4N$ (see Fig. 1). Within the Holstein-Primakoff approximation, we introduce the canonical variables $X_{\mathrm{I,II}} = J_{y,\mathrm{I,II}}/\sqrt{|\langle J_x\rangle|}$ and $P_{\mathrm{I,II}} = \pm J_{z,\mathrm{I,II}}/\sqrt{|\langle J_x\rangle|}$ [6]. The EPR entanglement condition [9,17] for such ensembles is given by $\xi = \Sigma_J/(2|\langle J_x\rangle|) = \mathrm{var}(X_{\mathrm{I}} - X_{\mathrm{II}})/2 + \mathrm{var}(P_{\mathrm{I}} + P_{\mathrm{II}})/2 < 1$, where $\Sigma_J = \mathrm{var}(J_{y,\mathrm{I}} - J_{y,\mathrm{II}}) + \mathrm{var}(J_{z,I} - J_{z,\mathrm{II}})$.

The entangling mechanism is due to the coupling to the x-polarized vacuum modes in the propagation direction z of the laser field (Fig. 1), which are shared by both ensembles and provide the desired common environment. Spin flip processes in the two samples accompanied by forward scattering result in indistinguishable photons leading to quantum interference and entanglement of the ensembles. These spin flips and the corresponding photon scattering (see level schemes in Fig. 1) are described by the interaction Hamiltonian of the type $H \propto \int_{\Delta\omega_{\mathrm{ls}}} d\mathbf{k}(Aa^\dagger_{\mathbf{k}} + A^\dagger a_{\mathbf{k}}) + \int_{\Delta\omega_{\mathrm{us}}} d\mathbf{k}(Ba^\dagger_{\mathbf{k}} + B^\dagger a_{\mathbf{k}})$, where the integrals cover narrow bandwidths centered around the lower and upper sideband at $\omega_L \mp \Omega$, respectively,

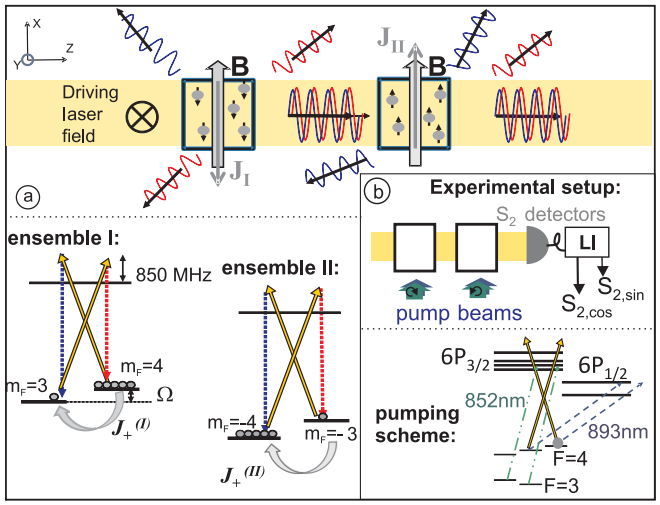

FIG. 1 (color). (a) Collective dissipation modes and atomic levels: two spatially separated atomic ensembles interact with the environment composed of the vacuum modes of the electromagnetic field. The coupling is driven by the y-polarized laser beam. The engineered collective dissipation is due to photons scattered in the forward z direction. Internal level scheme of the atoms: the effective two-level systems $|\uparrow\rangle$ and $|\downarrow\rangle$ are two magnetic sublevels Zeeman shifted by a magnetic field applied in the x direction, which defines the quantization axis. Atoms in the two ensembles are initialized in opposite spin states. The laser beam off-resonantly couples these levels to the excited states and to the electromagnetic vacuum modes. Because of the Zeeman shift of the ground state levels, photons are emitted into the upper and lower sidebands (shown in blue and red) leading to collective spin flips $J_\pm$. (b) Geometry of the experiment. The S_2 detector signal processed by the lock-in amplifier (LI) is used to determine the atomic quantum spin components $J_{y,z}$ as described in the text. The optical pumping scheme is also shown.

and with the nonlocal spin operators $A = \frac{1}{\sqrt{N}} \times (\mu J_{\mathrm{I}}^- - \nu J_{\mathrm{II}}^-)$, $B = \frac{1}{\sqrt{N}}(\mu J_{\mathrm{II}}^+ - \nu J_{\mathrm{I}}^+)$, where $\mu^2 - \nu^2 = 1$. The fact that the electromagnetic modes $a_{\mathbf{k}}^\dagger$ form a continuum is crucial for the entanglement to be created without measurements [12]. As emission into the forward direction is collectively enhanced for a large optical depth d [6], the forward scattered modes can successfully compete with spontaneous emission modes in directions other than z, which leads to decoherence of the atomic state. Note that the generation of entanglement cannot be explained by the interaction of photons emitted by the first ensemble with the second one, which is negligible in our parameter regime. The nonlocal dissipative atomic dynamics obtained after tracing over the photonic modes is governed by the master equation [12]: $\frac{d}{dt}\rho = d\frac{\Gamma}{2} \times (A\rho A^\dagger - A^\dagger A\rho + B\rho B^\dagger - B^\dagger B\rho + \mathrm{H.c.}) + \mathcal{L}_{\mathrm{noise}}\rho$, where ρ is the atomic density operator and Γ is the single atom radiative decay. The Lindblad terms in parentheses, which would usually describe regular spontaneous emission, drive the system into an EPR state with $\xi = (\mu - \nu)^2 < 1$ [12], due to the special nonlocal construction of A and B. $\mathcal{L}_{\mathrm{noise}}$ describes undesired processes such as single atom spontaneous emission, collisions, etc.

The experiments are performed using two dilute ^{133}Cs gas samples in 2.2 cm cubic cells separated by 0.5 m described elsewhere [6]. A bias magnetic field of 0.9 G leads to a Zeeman splitting of $\Omega = 2\pi \times 322$ kHz (see Fig. 1). The antirelaxation coating of the cell walls and careful magnetic shielding [14] provide the nonradiative decoherence time for populations and coherences of $T_1 \approx 130$ ms and $T_2 \approx 40$ ms. The two ensembles are initialized in the states $|4, \pm 4\rangle$ with orientation up to $P = 0.998(3)$ by applying a pump laser polarizing the $F = 4$ manifold and a laser repumping atoms from $F = 3$ to $F = 4$ for 10–50 ms [Fig. 1(b)]. The driving laser is blue detuned by 850 MHz from the $F = 4 \leftrightarrow F = 5$ transition of the D_2 line corresponding to $(\mu - \nu)^2 = 0.16$. The laser power influences both the collective and the single atom dissipation processes and has been optimized within a range of 5–15 mW. The nonlocal atomic state variance $\xi = \Sigma_J/(2|\langle J_x\rangle|)$ is inferred, and the entanglement condition $\xi < 1$ is verified by a local polarization measurement on the light transmitted through the two ensembles [Fig. 1(b)]. We use the same laser to create and to verify the entanglement which significantly simplifies the experiment. In the period $t < T$, up to a variable time T [see the pulse sequence in Fig. 2(b)] the laser serves only as the driving source for dissipation. The results of the measurements on the transmitted light are not used, which is equivalent to tracing out the light field. Beginning at $t = T$, the temporal mode of the transmitted light is used for the determination of the atomic state at time T using the established method [6,11,15,18] of linear mapping of the atomic state onto light (atomic tomography via quantum polarization spectroscopy). The particular linear mapping used here has been utilized in several other contexts [14,19,20] and is described by the input-output relations for atomic and light operators before and after the interaction:

$$\frac{1}{\sqrt{2}}(X_{\mathrm{I}}^{\mathrm{out}} - X_{\mathrm{II}}^{\mathrm{out}}) = e^{-\gamma_s T} \cdot \frac{1}{\sqrt{2}}(X_{\mathrm{I}}^{\mathrm{in}} - X_{\mathrm{II}}^{\mathrm{in}}) - \kappa(\mu - \nu)^2 y_{c+}^{\mathrm{in}},$$
$$y_{c-}^{\mathrm{out}} = y_{c+}^{\mathrm{in}} e^{-\gamma_s T} + \kappa \cdot \frac{1}{\sqrt{2}}(X_{\mathrm{I}}^{\mathrm{in}} - X_{\mathrm{II}}^{\mathrm{in}}), \qquad (1)$$

and similarly for $X_{\mathrm{I}} - X_{\mathrm{II}} \rightarrow P_{\mathrm{I}} + P_{\mathrm{II}}$ and $y_c \rightarrow y_s$. Here $\kappa^2 = (1 - e^{-2\gamma_s T})/(\mu - \nu)^2$ and $\gamma_s \propto (\mu - \nu)^2 J_x \Phi$, where Φ is the flux of photons in the drive field and T is the interaction time. The light operators are given by the $\cos(\Omega t)$ and $\sin(\Omega t)$ components of the Stokes operator S_2 weighted with an exponentially falling (rising) mode function: $y_{c-(+)}^{\mathrm{out(in)}} = \frac{1}{N_\pm\sqrt{S_x}} \int_0^T S_2^{\mathrm{out(in)}}(t)\cos(\Omega t) e^{\mp\gamma_s t} dt$ (analogously for sine modes). Just as the master equation does, the input-output relations predict an entangled atomic state with variance $\Sigma_J(t) \rightarrow (\mu - \nu)^2$, for $T \gg \gamma_s^{-1}$. For $(\mu - \nu)^2 \ll 1$ and finite $\gamma_s T$ the input-output relations reduce to the quantum-nondemolition type.

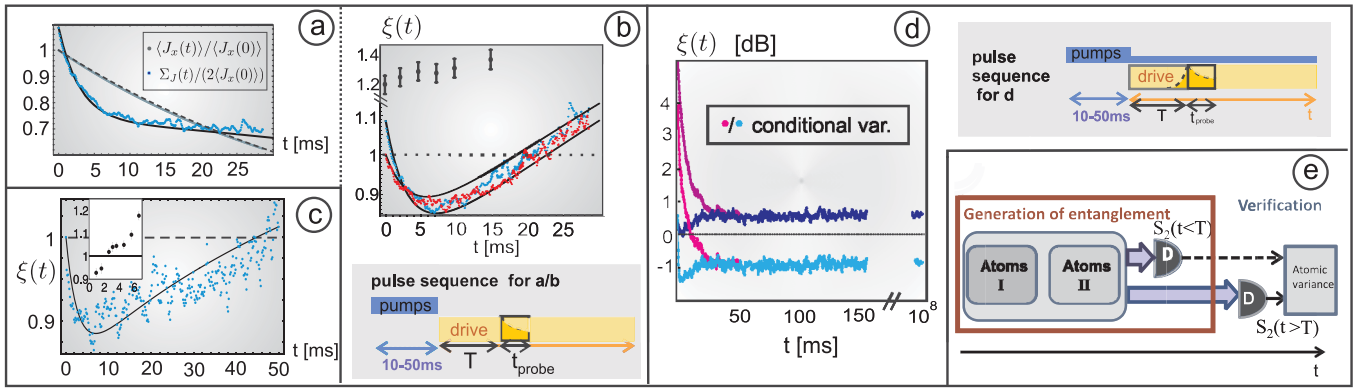

FIG. 2 (color). Entanglement generated by dissipation (a)–(c) and steady state entanglement (d). (a) Time evolution of $\Sigma_J(t)/(2|\langle J_x(t)\rangle|)$ (blue line) and $\langle J_x(t)\rangle/\langle J_x(0)\rangle$ (gray line). The theoretical fits (full and dashed black lines) are based on the parameters $d = 55$ (optical density), $\Gamma_{\rm col} = 0.002$ ms^{-1} (collisional rate), and $\tilde{\Gamma} = 0.193$ ms^{-1} (dephasing rate [22]). The rates for driving field induced transitions $|4, \pm 3\rangle \rightarrow |4, \pm 4\rangle$ and $|4, \pm 4\rangle \rightarrow |4, \pm 3\rangle$ are given by $\mu^2\Gamma$ and $\nu^2\Gamma$, respectively, where $\Gamma = 0.002$ ms^{-1}. (b) Entanglement $\xi(t)$ versus time in ms. Blue data points correspond to the results shown in (a). Data points in orange are obtained for a lower optical depth ($d = 35$). The other parameters used in the fits take the same values as in (a). $\xi(t) < 1$ certifies the creation of an inseparable state. The relevant pulse sequence is shown below. The data taken in the absence of the driving field (black points) show no entanglement. (c) Dissipative entanglement generation in the presence of the pump field which incoherently transfers atomic population from undesired levels within $F = 4$ back to the two-level subsystem. The pump rate is $\Gamma_{\rm pump} = 0.168$ ms^{-1}. $d = 37$, the fitting parameters $\Gamma_{\rm col}$ and Γ take the same values as in (a) and $\tilde{\Gamma} = 0.233$ ms^{-1}. The inset shows the evolution of $\xi(t)$ after the driving field is switched off after entanglement is generated by dissipation. (d) Entanglement $\xi(t)$ for different initial conditions. The upper curves show a purely dissipative evolution. The lower curves, the entanglement generated by dissipation combined with the measurement. Points on the right represent an average over measurements of 1 h where atoms were kept in a steady state. The used exponential time mode functions are depicted in the pulse sequence and are described in the text. (e) Schematic illustration of entanglement generation and verification. The signal from the detector D for times $t > T$ is used for verification of entanglement in (a)–(c). In (d) the signal taken at $t < T$ is given to the verifier as additional information.

The atomic EPR variance $\Sigma_J(T)$ at time T can be inferred by using the input-output relations (1). The Stokes operator S_2 [the photon flux difference between $+45°$ and $-45°$ polarizations with respect to the y axis in Fig. 1(b)] is measured in the time interval $[T; T + t_{\rm probe}]$ [see pulse sequence in Fig. 2(b)] with the photocurrent electronically processed to obtain the relevant light mode: $y_{c-}^{\rm readout} \propto \int_T^{T+t_{\rm probe}} S_2^{\rm out}(t)\cos(\Omega t)e^{-\gamma_s t}dt$. The parameters κ^2, γ_s, $(\mu - \nu)$ of the linear input-output relations are calibrated as described elsewhere [14,19]. The atomic state reconstruction is calibrated and verified carefully as described in detail in the Supplemental Material [21], where also the modification of the input-output equations by losses and decoherence is presented. We conclude that the measurement of ξ is reliable within the uncertainty of $\pm 4\%$ arising from uncertainty in the measurements of κ^2, the detection efficiency η. and the shot noise of light.

In the first set of experiments, entanglement is generated purely dissipatively. In the first series of this set, the pump and repump fields are turned off at time $t = 0$ [Figs. 2(a) and 2(b)] and the driving (entangling) laser is turned on. In the presence of the drive field ($P \approx 5.6$ mW) T_2 is reduced to 6 ms and T_1 to 34 ms. This decoherence has been considered the fundamental limitation for the entanglement generated by measurements [6]. Here, the collective entangling dissipation due to forward scattering dominates over the single atom decoherence and leads to a rapid reduction of $\Sigma_J(t)$ on the time scale of γ_s^{-1}. Figure 2(a) shows the time evolution of $\Sigma_J(t)$ normalized to $2|\langle J_x(0)\rangle|$. For a coherent spin state (CSS) $\xi = 1$, and $\Sigma_{\rm CSS} = 2|\langle J_x\rangle|$ defines the projection noise (PN) level, below which lies the noise level of entangled states. The dynamics of $2|\langle J_x(t)\rangle|$ due to single atom spontaneous emission and collisions on the slow time scale of T_1 is also shown in Fig. 2(a). Figure 2(b) presents the time evolution of entanglement for two values of the optical depth $d \approx 34$ ($\Theta = 8.5°$ [21]) and $d \approx 56$ ($\Theta = 14.0°$). The data are well fitted with theory [12] using the collisional rate $\Gamma_{\rm col}$ and dephasing rate $\tilde{\Gamma}$ [22] compatible with experimental values. The details of calculations of the fits are given in [21]. The time interval 0.015 s over which entanglement is continuously maintained is several times longer than the best previous results obtained for measurement induced entanglement [5,6] and much longer than T_2. For comparison, if the driving (entangling) laser is off during $0 < t < T$ and is turned on only at $t = T$ to measure the atomic state, $\xi(T)$ predictably stays above the PN level [black points in Fig. 2(b)]. Also, a slight deliberate mismatch of the Larmor frequencies of the two ensembles in the preparation period by $\sim$20 Hz leads to the disappearance of the entanglement. This can be viewed as a direct consequence of the "which way" information due to the distinguishability of photons emitted by the two ensembles.

In the series presented above, entanglement is created in a quasisteady state rather than in a steady state, as would be the case for atoms with a true two-level atomic ground state, for example, in ytterbium ensembles [23]. On the time scale of T_1, atoms are lost to other magnetic sublevels of $F = 4$ and to the level $F = 3$. This causes the eventual extinction of entanglement as described well by the theoretical fits shown in Figs. 2(a) and 2(b) with the pumping rate Γ_{pump} being close to the experimental value. In the next series of experiments, the pumping field of an optimal strength resonant with the $F = 4$ state is kept on during the entanglement generation period $t > 0$ [Fig. 2(c)]. Remarkably, this incoherent process does not suppress generation of entanglement, but on the contrary brings it further towards a steady state. The entanglement can now be maintained for 0.04 s thanks to pumping atoms from sublevels $|m_F| \leq 3$ which contribute higher noise, back to $|m_F| = 4$ which is a dark state for the pump beam. The eventual loss of entanglement is in part due to atoms which are lost to the $F = 3$ ground state, effectively reducing d. If the entangling mechanism is turned off, the entangled state decays in 2 ms [inset in Fig. 2(c)], as expected [6] from the decoherence in the dark.

Finally, we demonstrate generation of steady state atomic entanglement. To this end, a repumping field $F = 3 \rightarrow F = 4$ is added during the entanglement generation, thus closing down the last escape channel from the relevant spin system. The atoms reach a steady state which is, however, not entangled because the collective processes are not sufficiently strong to overcome the noise added by the incoherent repumping field. Theory predicts [12] that a steady state entanglement can be achieved for $d = 100$, but this is experimentally unfeasible. However, we can use the fact that, due to single atom decoherence sources, the atomic state is not pure, and hence forward scattered light is not completely disentangled from the atoms. Up to now, measurements on light variables have only been used to verify entanglement at time T for which only $y^{\mathrm{out}}_{c,s-}(t > T)$ have been utilized. Using the results of the continuous measurement on the open atomic quantum system during the interval $t < T$, we can enhance the entanglement generated by dissipation and maintain it in the steady state. In this scenario, the verifier [Fig. 2(e)] receives the classical information $S^{\mathrm{out}}_2(t < T)$ which is used to calculate the conditional variance $\mathrm{var}(y^{\mathrm{cond}}_{c,s}) = \mathrm{var}(y^{\mathrm{readout}}_{c,s}(T) - \alpha y^{\mathrm{feed}}_{c,s}(t < T)$. Here, $y^{\mathrm{feed}}_{c}(t < T) = \frac{1}{N_f\sqrt{S_x}} \int_0^T S^{\mathrm{out}}_2(t) \cos(\Omega t) e^{\gamma_m t} dt$ and the feedback gain α and the time constant γ_m are optimized to achieve maximal noise reduction. The light mode that brings about the best noise reduction is a fast growing exponential mode, with $\gamma_m = 0.83\ \mathrm{ms}^{-1} > \gamma = 1/T_2 = 0.27\ \mathrm{ms}^{-1}$. The conditionally reduced atomic variance $\xi_{\mathrm{cond}} = \mathrm{var}[\frac{1}{2}(X_{\mathrm{I}} - X_{\mathrm{II}}) + \frac{1}{2}(P_{\mathrm{I}} - P_{\mathrm{II}}) - \frac{\alpha}{\kappa}(y^{\mathrm{feed}}_{c} + y^{\mathrm{feed}}_{s})(t < T)]$ is then found from $\mathrm{var}(y^{\mathrm{cond}}_{c,s})$ using the same calibrated input-output relations as above. These central results are displayed in Fig. 2(d), which shows the evolution of the variances of the purely dissipatively generated atomic state (upper curves) and the entanglement produced using the hybrid method including dissipation and continuous measurements (lower curves). Each pair of curves is taken with two different initial conditions. These results demonstrate a very important aspect of our work—they show that the generated steady state is independent of the initial state, and that entanglement is maintained for up to an hour, if dissipative processes are combined with measurements.

In conclusion, we have observed entanglement of macroscopic atomic ensembles generated by dissipation and the steady state atomic entanglement. The results present a new step in quantum control of entanglement. Dissipatively generated entanglement provides not only event-ready entangled links for standard protocols but is also an elementary resource for future applications in continuous quantum information processing schemes, such as dissipative distillation and repeater protocols, which allow for the distribution of long-range high-quality steady state entanglement [7].

We acknowledge support from the Elite Network of Bavaria (ENB) project QCCC and the EU projects COMPAS, *Q*-ESSENCE, and QUEVADIS. C. A. M. acknowledges valuable discussions with K. Hammerer, K. G. H. Vollbrecht, and G. Giedke.

*Current address: Institute of Experimental Physics, University of Warsaw, Warsaw, Poland.
†polzik@nbi.dk

[1] C. Myatt *et al.*, Nature (London) **403**, 269 (2000); S. Gleyzes *et al.*, Nature (London) **446**, 297 (2007); S. Hofferberth *et al.*, Nature (London) **449**, 324 (2007); M. Branderhorst *et al.*, Science **320**, 638 (2008); N. Syassen *et al.*, Science **320**, 1329 (2008); J. Barreiro *et al.*, Nature (London) **470**, 486 (2011); R. Bloomer, M. Pysher, and O. Pfister, New J. Phys. **13**, 063014 (2011).

[2] J. F. Poyatos, J. I. Cirac, and P. Zoller, Phys. Rev. Lett. **77**, 4728 (1996).

[3] M. B. Plenio and S. F. Huelga, Phys. Rev. Lett. **88**, 197901 (2002); B. Kraus and J. I. Cirac, Phys. Rev. Lett. **92**, 013602 (2004); S. Diehl *et al.* Nature Phys. **4**, 878 (2008); F. Verstraete, M. M. Wolf, and J. I. Cirac, Nature Phys. **5**, 633 (2009); J. T. Barreiro *et al.*, Nature (London) **470**, 486 (2011); A. S. Parkins, E. Solano, and J. I. Cirac, Phys. Rev. Lett. **96**, 053602 (2006).

[4] L.-M. Duan *et al.*, Nature (London) **414**, 413 (2001).

[5] H. J. Kimble, Nature (London) **453**, 1023 (2008).

[6] K. Hammerer, A. S. Sørensen, and E. S. Polzik, Rev. Mod. Phys. **82**, 1041 (2010).

[7] K. G. H. Vollbrecht, C. A. Muschik, and J. I. Cirac, arXiv:1011.4115.

[8] First results demonstrating the creation of entanglement by dissipation are reported in H. Krauter, C. A. Muschik,

K. Jensen, W. Wasilewski, J. M. Petersen, J. I. Cirac, and E. S. Polzik, arXiv:1006.4344.
[9] B. Julsgaard, A. Kozhekin, and E. S. Polzik, Nature (London) **413**, 400 (2001).
[10] D. N. Matsukevich *et al.*, Phys. Rev. Lett. **96**, 030405 (2006); C. W. Chou *et al.*, Nature (London) **438**, 828 (2005); M. Eisaman *et al.* Nature (London) **438**, 837 (2005); Z. Yuan *et al.* Nature (London) **454**, 1098 (2008).
[11] J. Appel *et al.*, Proc. Natl. Acad. Sci. U.S.A. **106**, 10 960 (2009).
[12] C. A. Muschik, E. S. Polzik, and J. I. Cirac, Phys. Rev. A **83**, 052312 (2011).
[13] A. Furusawa and N. Takei, Phys. Rep. **443**, 97 (2007).
[14] W. Wasilewski *et al.*, Phys. Rev. Lett. **104**, 133601 (2010).
[15] M. H. Schleier-Smith, I. D. Leroux, and V. Vuletić, Phys. Rev. Lett. **104**, 073604 (2010).
[16] C. Gross *et al.*, Nature (London) **464**, 1165 (2010); M. F. Riedel *et al.*, Nature (London) **464**, 1170 (2010).
[17] L.-M. Duan *et al.*, Phys. Rev. Lett. **84**, 2722 (2000).
[18] M. Koschorreck *et al.*, Phys. Rev. Lett. **105**, 093602, (2010).
[19] W. Wasilewski *et al.*, Opt. Express **17**, 14 444 (2009).
[20] K. Jensen *et al.*, Nature Phys. **7**, 13 (2010).
[21] See Supplemental Material at http://link.aps.org/supplemental/10.1103/PhysRevLett.107.080503 for a description of calibration procedures and fit parameters.
[22] The effective dephasing rate associated with noise effects $\tilde{\Gamma} = \Gamma_{\mathrm{cool}} + \Gamma_{\mathrm{heat}} + \Gamma_{\mathrm{deph}}$ includes the effective single particle cooling rate Γ_{cool} (which is a sum of rates corresponding to cooling processes due to the driving and pump field and collisions), the effective single particle heating rate $\Gamma_{\mathrm{heat}} = \Gamma_{\uparrow\downarrow} = \nu^2\Gamma + \gamma_{\mathrm{col}}$, as well as pure dephasing Γ_{deph}.
[23] T. Takano *et al.*, Phys. Rev. Lett. **102**, 033601 (2009).